Obour Institute Journal
for Engineering and Technology (OI-JET)
Journal homepage: https://oijet.journals.ekb.eg
Volume (1), Issue (1), December 2023

Fortifying of Reinforced Concrete Beams Utilizing Near Surface Mounted FRP

Open access

Khaled F. Khalil: Professor Structural Eng. Dept., Faculty of Eng., Zagazig University, Zagazig, Egypt, Vice Dean, High Institute for Engineering and Technology Al-Obour (K21 Cairo /Bilbies Road), Higher Education Ministry, Cairo, Egypt, Khaledfawzy@oi.edu.eg
Mahmoud Nasr, Teaching Assistant, Civil Engineering Department, High Institute for Engineering and Technology at Al - Obour (K21 Cairo /Bilbies Road),Higher Education Ministry, Cairo, Egypt, mahmoud.nasr@oi.edu.eg
Azza I. Anan: Civil Engineering Department, High Institute for Engineering and Technology at Al - Obour (K21 Cairo /Bilbies Road),Higher Education Ministry, Cairo, Egypt, azza.anan@oi.edu.eg

Received August 10, 202٣, Revised September 5, 202٣, Accepted September 15, 202٣

Abstract

The restoration and fortifying of supported substantial individuals utilizing Near to Surface Mounted (NSM) method has demonstrated its prosperity and becoming famous in the realm of development. The NSM strategy utilizing carbon, aramid, and glass fiber supported polymers (FRP) bars has drawn in the consideration of numerous analysts during the last many years. This paper presents numerical analysis of the way of behaving of reinforced beams with Three kinds of FRP; carbon fiber bar (CFRP), aramid fiber bar (AFRP), and glass fiber bar (GFRP) in flexural. Three-dimensional finite element beam models are made on the limited component programming ANSYS-2019 to study the flexural reaction of the researched models. The built non-straight limited component models were confirmed by the exploratory work results that are accessible in reference. A parametric report was led to inspect the impact of type, number, width of NSM FRP bars, and bond length on the flexural reaction and extreme burden conveying limit of the fortified beams. A portion of the concentrated-on boundaries impacted the strength capacity, stiffness, ductility, and energy absorption of the beam models.

***KEYWORDS**: RC beams, Shear, Repair, Rectangular opening, FRP, Nonlinear, FEA, ANSYS*

1. Introduction

Strengthening and repair of reinforced concrete structures have been among the most important challenges in structure engineering. Furthermore, the cost of rehabilitation and repair in most cases is far less than the cost of replacement and thus reducing service interruption time (M. Tavakkolizadeh, 2001). The main reasons for strengthening a structure; (1) enhance load caring capacity, (2) to reduce deflection at a service loading, and (3) to control width and distribution of cracks (Hollaway M.A. and Raoof M, 2001).

The early methods for strengthening and repairing of reinforced concrete structures have been used in Europe since the 1950 by using near surface mounted steel rods (S.O. Asplund, 1949), however the use of steel bars in NSM method has resulted in several disadvantages including difficulty in handling at site and possibility of corrosion at the adhesive-steel interface. Also externally bonded systems have shown their effectiveness in strengthening RC structures. The use of bonded steel plates and bars for the strengthening and rehabilitation of RC structures has been popular for many years [4]. Recently, the use of externally bonded fiber reinforced polymer laminates has

Correspondence Author Khaled F. Khalil Khaledfawzy@oi.edu.eg
Copyrights ©, High Institute of Engineering and Technology Al Obour
Print ISSN, 2974-4539, Online ISSN: 3062-5270

been one of the most attractive methods for strengthening reinforced concrete and a large number of research and practical projects have been undertaken [(S. Yang, K.Park, and W. Neale, 2009) (J. F. Chen and J. G. Teng. 2001) (M. Tavakkolizadeh, 2001)]. More recently, the near surface mounted (NSM) FRP has become an attractive method for strengthening RC members and masonry, thus increasing flexural and shear strength.

The advantages of FRP versus steel as NSM reinforcement are better corrosion resistance, ease and speed of installation due to its light weight, and smaller groove size due to the higher tensile strength. Compared to externally bonded FRP reinforcement, the NSM system has a number of advantages [(L. De Lorenzis and J.G. Teng, 2007) (R.Parretti and A. Nanni, 2004)]: (a) NSM FRP technique does not require extensive surface preparation work, and after groove cutting, requires minimal installation time compared to externally bonded FRP laminates. (b) NSM reinforcement is protected by the concrete cover and so are less exposed to accidental impact and mechanical damage, fire, and vandalism; this aspect makes this technology particularly suitable for the strengthening and repairing of negative moment regions of beams and slabs. (c) NSM reinforcement is less prone to debonding from the concrete substrate; (d) the aesthetics of a strengthened structure with NSM reinforcement are virtually unchanged.

2. Literature Review

Many studies on the use of NSM FRP for flexural and shear strengthening of RC beams have been published. (Kang J. Y., rt al., 2005) performed an experimental investigation on the flexural behavior of RC beams strengthened with NSM CFRP reinforcement. Two amounts of CFRP strips were examined, namely 21 mm2 and 35 mm2, they reported that the NSM strengthened specimens utilized the CFRP reinforcement more efficiency than those of externally bonded strengthened beams. (De Lorenzis L., Nanni A., and La Tegola, 2000) used FRP bars as a near surface mounted for shear and flexural strengthening, their test results showed that for flexural strengthened RC beams, an increase of 44% of the ultimate strength compared to that of the control beam. (EL – Hacha R., et al., 2004) conducted a study on the flexural strengthening of RC beams using NSM FRP technique. Various variables were examined: number of the FRP rod/strip, form of FRP: strip/rod and type of FRP: glass and carbon, they found in their study that using NSM reinforcement for flexural strengthening with CFRP strips has a higher load carrying capacity than those of the CFRP rod for the same axial stiffness. Such result was explained as a possibility of an early de-bonding that occurred between the CFRP rod and epoxy interface. (Sabau C., et al., 2018) investigated the efficiency of side mounted (S) compared to bottom mounted (B) NSM bars to prevent concrete cover detachment (CCD). Compared to B-NSM, the S-NSM solution was successful in avoiding brittle CCD failure and showed increased rotational capacity and energy dissipation at failure. Existing CCD debonding models were found to be conservative. (Szczech D., Krawczyk L. and Kotynia R, 2020) conducted a study on the reinforced concrete beams flexurally strengthened with Carbon Fibre Reinforced Polymer (CFRP) laminates using the Near Surface Mounted (NSM) technique, in this research three beams were tested, the first specimen was a reference beam without any strengthening, the second was strengthened under the self-weight and the third beam was strengthened under initial preloading equal to 83% of the ultimate load of the reference beam, High strengthening efficiency of the NSM strengthening was confirmed by 109% and 130% when compared with the non-strengthened beam, respectively for the first and the second beam. (N. Jeevan et al. 2023) make a study on the flexural strength in RC beams using Near Surface Mounted (NSM) technique, by considering the orientation of laminate as the main priority in NSM strengthening, the strengthening methodologies adopted in this research work are Near Surface Mounted Laminate with Vertical Orientation (NSMLV), Near Surface Mounted Laminate with Vertical Orientation having Anchorages (NSMLVA) and Near Surface Mounted Laminate with Horizontal Orientation (NSMLH), all strengthened beams showed improved ultimate loads by satisfying the serviceability requirement. The ultimate load shows an increase of 21.74 %, 40.22%

and 71.74% for NSMLV, NSMLVA and NSMLH technique respectively compared to control beams.

The main objective of this research is to study Numerically the behavior of NSM strengthening with different types of FRP bars, such as carbon fiber (CFRP), aramid fiber (AFRP), and glass fiber (GFRP). Also parametric study is performed to examine the effects of the bond length, bar type, and diameter on some important structural properties; such as stiffness, ductility and energy absorption of the beam models.

3. Nonlinear Finite Element Analysis

In this paper, ANSYS- 2019 finite element program is used for analysis. The concrete damaged plasticity model in ANSYS provides a general capability for modeling concrete in all types of structures using concepts of isotropic damaged elasticity in combination with isotropic tensile and compressive plasticity to represent the inelastic behavior of concrete. The SOLID 65 element was used to model the concrete, this element has eight nodes with three degrees of freedom at each node – translations in the nodal x, y, and z directions, this element is capable of plastic deformation, cracking in three orthogonal directions, and crushing. LINK180 element was used to model steel and CFRP tendons, this element is a 3D spar element and it has two nodes with three degrees of freedom – translations in the nodal x, y, and z directions, the element is also capable of plastic deformation.

3.1 Verification of the Nonlinear Finite Element Modeling

To verify the nonlinear finite element modeling constructed by the use of the nonlinear finite element analysis program ANSYS. A seven models, which are identical to those tested experimentally by (S.M. Soliman, E. El-Salakawy & B. Benmokrane, 2008) are prepared and constructed by the program, their results are compared to those obtained experimentally to check the validity of the finite element modeling. Figure (1) shows the dimension and the reinforcement details for the strengthened tested beams with NSM FRP bars. The beams were tested in four-point bending over a simply supported clear span of 2600 mm with shear span equal (3.02). A 500 kN closed-loop MTS actuator was used to apply the load, the rate of loading was 0.02 mm/sec up to failure.

Model B0 was tested as a control specimen to obtain the capacity of the un-strengthened beams, with dimensions 3010 mm long, 200 mm-wide and 300 mm-deep. Two steel bars with 10mm diameter were used in the bottom and top of this beam. Two-legged 8-mm diameter steel stirrups spaced at 100 mm over the whole length of the beam were used to avoid any shear failure.

Model B1 to B4 have the same properties of model B0, but each beam is strengthened with one 9.5 mm-diameter CFRP bar inside a square groove (19 mm). The test parameter in this series is the bonded length; 12d, 24d, 48d and 60d for B1, B2, B3, and B4, respectively, where d is the bar diameter.

Model B5 and B6 have the same properties of model B0 and strengthened with 12.7 mm- diameter CFRP and GFRP bar inside a square groove (25.4 mm) at 48d bonded lengths for the two beams.

Deflections and load capacities of experimental models vs. finite element models at ultimate Load with differences in percentage were shown at Table (1) and Figure (2). It is seen that the FEM models provided good predictions against the experimental data, including maximum errors of 13.52%, and 16.00% for the ultimate loads and the maximum deflection, respectively.

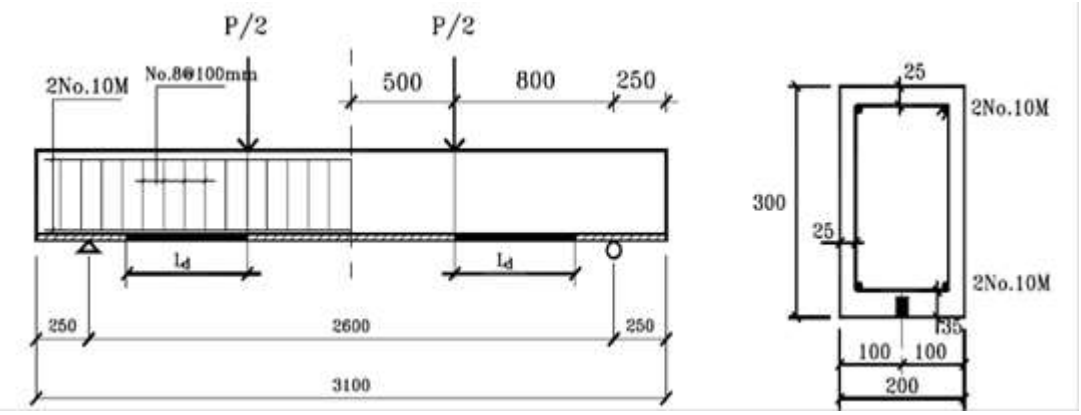

Fig (1) Dimensions and reinforcement details of the tested beams

Table (1) Deflections and Load Capacities of Experimental versus Finite Element Models

Beam No.	Experimental data		Analytical data		Difference percentage	
	Ultimate Load (kN)	Maximum deflection (mm)	Ultimate Load (kN)	Maximum deflection (mm)	Load %	Deflection %
B0	55.00	75.89	54.66	83.10	0.62%	9.50%
B1	66.89	17.20	68.00	16.90	1.66%	1.74%
B2	72.64	25.38	79.00	22.80	8.76%	11.30%
B3	93.87	23.97	93.60	27.40	0.30%	14.30%
B4	96.37	26.80	96.00	31.09	0.38%	16.00%
B5	108.00	19.00	102.50	18.90	5.40%	0.53%
B6	112	49.36	98.66	47.20	13.52%	4.58%

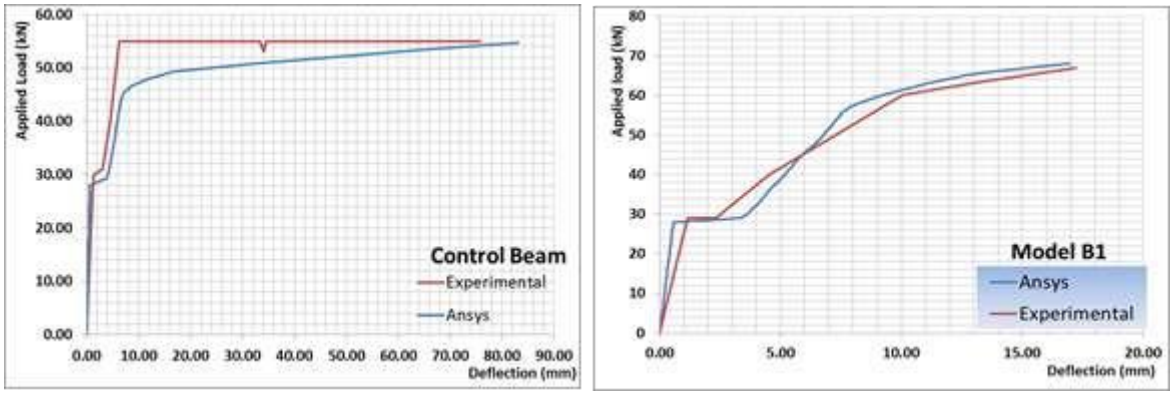

Fig (2) load deformation responses for B0 and B1

3.2 Parametric study

In this numerical study all models were rectangular (200 mm × 300 mm) with length 3100
mm. 52 specimens of a rectangular RC beams were strengthened with different types of fiber carbon (CFRP), aramid fiber (AFRP) and glass fiber (GFRP). The models include 36 specimens strengthened with one bar CFRP, AFRP and GFRP with different diameter 9.50, 12.70, and 16.00 mm having bond length 12d, 24d, 48d, and 60d. The other models include 16 specimens strengthened with two and three bars CFRP and GFRP with 9.50mm diameter and having bond length 12d, 24d, 48d, and 60d, Table (3) show the study model details.

The properties of the steel and FRP reinforcing bars used in this study are listed in Table (2). An epoxy adhesive type (HIT RE 500) was used in this study. The HIT RE 500 is a high strength two-part epoxy based adhesive and can be applied on wet or dry surfaces, it is specially designed for fastening into solid base materials in a wide range of material temperatures (49o C down to -5o C). The tensile strength and modulus of elasticity of the HIT RE 500 adhesive are 43.5 and 1493 MPa, respectively.

Table (2) Material properties

Bar type	Bar diameter (mm)	Modules of elasticity (GPa)	Tensile Strength (MPa)	Ultimate strain %
CFRP	9.5,12.7,16.00	122 134	1536±18 986±50	1.22±0.07 0.74±0.05
GFRP	9.5,12.7,16.00	42	749±27	1.80±0.04
AFRP	9.5,12.7,16.00	70	1300±15	1.90±0.05
Steel	11.3	200	F_y=454 F_u=571	0.23

Table (3) study model details

Model	Type of FRP	Diameter of FRP	No. of bars	Groove width	Bonded length
BC1	Carbon	9.50 mm	1	2d (19 mm)	12d
BA1	Aramid	9.50 mm	1	2d (19 mm)	12d
BG1	Glass	9.50 mm	1	2d (19 mm)	12d
BC5	Carbon	12.70 mm	1	2d (25.40 mm)	12d
BA5	Aramid	12.70 mm	1	2d (25.40 mm)	12d
BG5	Glass	12.70 mm	1	2d (25.40 mm)	12d
BC9	Carbon	16.00 mm	1	2d (32.00 mm)	12d
BA9	Aramid	16.00 mm	1	2d (32.00 mm)	12d
BG9	Glass	16.00 mm	1	2d (32.00 mm)	12d
BC2	Carbon	9.50 mm	1	2d (19 mm)	24d
BA2	Aramid	9.50 mm	1	2d (19 mm)	24d
BG2	Glass	9.50 mm	1	2d (19 mm)	24d
BC6	Carbon	12.70 mm	1	2d (25.40 mm)	24d
BA6	Aramid	12.70 mm	1	2d (25.40 mm)	24d
BG6	Glass	12.70 mm	1	2d (25.40 mm)	24d
BC10	Carbon	16.00 mm	1	2d (32.00 mm)	24d
BA10	Aramid	16.00 mm	1	2d (32.00 mm)	24d
BG10	Glass	16.00 mm	1	2d (32.00 mm)	24d
BC3	Carbon	9.50 mm	1	2d (19 mm)	48d
BA3	Aramid	9.50 mm	1	2d (19 mm)	48d
BG3	Glass	9.50 mm	1	2d (19 mm)	48d
BC7	Carbon	12.70 mm	1	2d (25.40 mm)	48d
BA7	Aramid	12.70 mm	1	2d (25.40 mm)	48d
BG7	Glass	12.70 mm	1	2d (25.40 mm)	48d
BC11	Carbon	16.00 mm	1	2d (32.00 mm)	48d

Cont. Table (3) study model details

Model	Type of FRP	Diameter of FRP	No. of bars	Groove width	Bonded length
BA11	Aramid	16.00 mm	1	2d (32.00 mm)	48d
BG11	Glass	16.00 mm	1	2d (32.00 mm)	48d
BC4	Carbon	9.50 mm	1	2d (19 mm)	60d
BA4	Aramid	9.50 mm	1	2d (19 mm)	60d
BG4	Glass	9.50 mm	1	2d (19 mm)	60d
BC8	Carbon	12.70 mm	1	2d (25.40 mm)	60d
BA8	Aramid	12.70 mm	1	2d (25.40 mm)	60d
BG8	Glass	12.70 mm	1	2d (25.40 mm)	60d
BC12	Carbon	16.00 mm	1	2d (32.00 mm)	60d
BA12	Aramid	16.00 mm	1	2d (32.00 mm)	60d
BG12	Glass	16.00 mm	1	2d (32.00 mm)	60d
BC13	Carbon	9.50 mm	2	2d (19.00 mm)	12d
BG13	Glass	9.50 mm	2	2d (19.00 mm)	12d
BC14	Carbon	9.50 mm	2	2d (19.00 mm)	24d
BG14	Glass	9.50 mm	2	2d (19.00 mm)	24d
BC15	Carbon	9.50 mm	2	2d (19.00 mm)	48d
BG15	Glass	9.50 mm	2	2d (19.00 mm)	48d
BC16	Carbon	9.50 mm	2	2d (19.00 mm)	60d
BG16	Glass	9.50 mm	2	2d (19.00 mm)	60d
BC17	Carbon	9.50 mm	3	2d (19.00 mm)	12d
BG17	Glass	9.50 mm	3	2d (19.00 mm)	12d
BC18	Carbon	9.50 mm	3	2d (19.00 mm)	24d
BG18	Glass	9.50 mm	3	2d (19.00 mm)	24d
BC19	Carbon	9.50 mm	3	2d (19.00 mm)	48d
BG19	Glass	9.50 mm	3	2d (19.00 mm)	48d
BC20	Carbon	9.50 mm	3	2d (19.00 mm)	60d
BG20	Glass	9.50 mm	3	2d (19.00 mm)	60d

4. Results and Discussions

4.1 Cracks Patterns

The failure modes were ductile failure, and varied with changing bond length. It can be observed that by increasing the bond length from 12d to 60d, the cracks increase, spread, and start to appear on the compression zone of the beam specimens as shown in Figure 3. Also, the Figure 3 shows the spread of cracks increases with the decrease of modules of elasticity of FRP bars. The spread of cracks in carbon specimens is less than both aramid and glass specimens due to higher modules of elasticity of carbon than glass and aramid. In glass and aramid specimens at 12d bond length, a few cracks start to appear in the compression zone of the beam specimen.

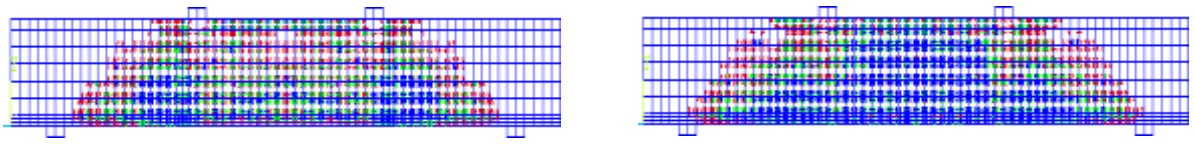

Bond length =12d (Glass-9.50mm)

Bond length =60d (Glass-9.50mm)

Fig (3) cracks patterns

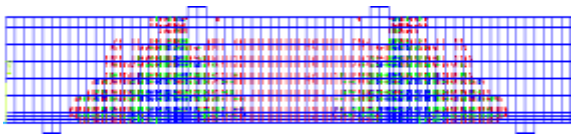

Bond length =12d (Carbon-16.00mm)

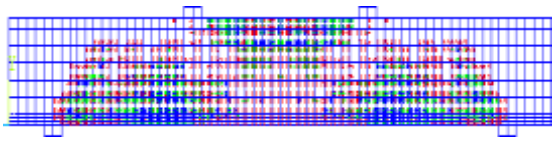

Bond length =60d (Carbon-16.00mm)

Continues of figure (3) cracks patterns

4.2 Effect of Type and Diameter of NSM FRP Bars

The results are shown in Table 4 and Figure 4 to Figure 7, where (Pcr , Δcr), (Py , Δy), and (Pu , Δu), which are the coordinates of first cracking point, elastic limit point (or yield), and ultimate point, respectively are given. Using information gained from load-deflection relations, the ductility index (μΔ), the initial un-cracked elastic stiffness (Ki), and the energy absorption index (E.A.I = the ratio of total area under load-deflection curve to area under elastic part at the same curve) are listed in Table 5. They are calculated from the following equations.

$$\mu_{\Delta} = \Delta_u / \Delta_y \quad \text{.....(1)}$$

$$K_i = P_{cr} / \Delta_{cr} \quad \text{.....(2)}$$

Table (4) load-deflection values for 12d, 24d, 48d, and 60d bond length

Bond length	Model	P_{cr} (kN)	Δ_{cr} (mm)	P_y (kN)	Δ_y (mm)	P_u (kN)	Δ_u (mm)
-	**B0**	28.5	2	47	8.6	54.67	83.18
	BC1	28.5	2	58	8	68	16.9
	BA1	28	2	54	7.5	69	21.63
	BG1	27.5	2	53	7.8	68	29.5
	BC5	28.5	1.9	62	7.5	71	12.9
	BA5	28	2	58	7.5	72	17.45
	BG5	27	1.9	55	7.5	70.66	19.5
	BC9	28.5	1.6	65	7.5	75	12.99
	BA9	28	1.9	64	8	75	15.48
12d	**BG9**	27.5	1.9	58	8	75	19.6
	BC2	28.5	2	56	7.5	79	22.8
	BA2	28	2	55	7.5	79	33.9
	BG2	27	2	53	7.5	72	35.5
	BC6	29	1.6	70	8.2	86.86	15.9
	BA6	28.5	2	59	8	83	21.17
	BG6	27	1.9	55	8	72	21.9
	BC10	29	1.6	86	9	104	16.7
	BA10	28.5	1.9	69	8	100	20.85
24d	**BG10**	27.5	1.9	62	8	94	33.4

Cont. Table (4) load-deflection values for 12d, 24d, 48d, and 60d bond length

Bond Length	Model	P_{cr} (kN)	Δ_{cr} (mm)	P_y (kN)	Δ_y (mm)	P_u (kN)	Δ_u (mm)
	BC3	28.5	2	58	7.5	93.6	27.4
	BA3	27.5	2	55	7.5	88	40.44
	BG3	27	2	55	7.5	82.66	53.4
	BC7	28.5	1.5	74	8	102.5	18.9
	BA7	29	2	61	7.8	98	38.61
	BG7	27.5	2	56	8	96	43.2
	BC11	28.5	1.4	86	8	107	27.6
	BA11	28	1.9	73	8	102	37.12
48d	**BG11**	28	2	62	8	98.4	37.5
	BC4	28.5	2	60	8	96	31.09
	BA4	27.5	2	55	7.5	92	56.9
	BG4	27	2	55	7.5	92	64.7
	BC8	28	1.5	76	8	105	23.3
	BA8	28	2	61	7.5	100	50.51
	BG8	27	2	56	8.5	96	59.8
	BC12	28.5	1.4	91	8.5	120	36.1
	BA12	27.5	1.8	71	8	107	39.01
60d	**BG12**	27.5	1.9	64	8	105	39.14
	BC13	27.5	1.6	63	7.5	70	12.2
	BG13	27	1.7	55	7.8	70	18.2
	BC17	27.5	1.5	63	6.5	69	11.4
12d	**BG17**	26.5	1.8	60	8	70	16.8
	BC14	27.5	1.5	74	8	84	16.9
	BG14	27	1.8	56	7.5	80	28.03
	BC18	28	1.5	74	7.8	83	14.4
24d	**BG18**	26.5	1.8	60	8	83	23.7
	BC15	27.5	1.5	76	8	102	21.7
	BG15	27.5	1.9	58	8	94	38.6
	BC19	27.5	1.3	87	8	114.67	20.5
48d	**BG19**	26.5	1.8	61	8	96	33.9
	BC16	27.5	1.6	80	8.5	108	24.6
	BG16	27.5	1.9	58	8	95	56.9
	BC20	28	1.3	90	8	115	22.4
60d	**BG20**	26.5	1.8	61	8	98	36.26

Table (5) Computed data at 12d, 24d, 48d, and 60d bond length

Bond length	Model	E.A.I	μΔ	Ki
-	**B0**	13.22	9.67	14.25
	BC1	3.1	2.11	14.25
	BA1	3.61	2.88	14
	BG1	6.65	3.78	13.75
	BC5	2.2	1.72	15
	BA5	3.4	2.33	14
	BG5	3.57	2.6	14.21
	BC9	2.32	1.73	17.81
	BA9	2.67	1.94	14.74
12d	**BG9**	3.74	2.45	14.47
	BC2	4.74	3.04	14.25
	BA2	7.42	4.52	14
	BG2	8.37	4.73	13.5
	BC6	2.9	1.94	18.13
	BA6	4.52	2.65	14.25
	BG6	5.04	2.74	14.21
	BC10	2.62	1.86	18.13
	BA10	4.41	2.61	15
24d	**BG10**	7.66	4.18	14.47
	BC3	6.62	3.65	14.25
	BA3	10.07	5.39	13.75
	BG3	14.4	7.12	13.5
	BC7	4.01	2.36	19
	BA7	9.95	4.95	14.5
	BG7	11.5	5.4	13.75
	BC11	6	3.45	20.36
	BA11	8.1	4.64	14.74
48d	**BG11**	9.51	4.69	14
	BC4	7.85	3.89	14.25
	BA4	15.85	7.59	13.75
	BG4	19.9	8.63	13.5
	BC8	4.9	2.91	18.67
	BA8	14.88	6.73	14
	BG8	16.21	7.04	13.5
	BC12	8.06	4.25	20.36
	BA12	10.04	4.88	15.28
60d	**BG12**	10.7	4.89	14.47
	BC13	1.98	1.63	17.19
	BG13	3.52	2.33	15.88
	BC17	2.01	1.75	18.33
12d	**BG17**	3.02	2.1	14.72

Conti. Table (5) Computed data at 12d, 24d, 48d, and 60d bond length

Bond length	Model	E.A.I	μΔ	Ki
12d	**BC13**	1.98	1.63	17.19
	BG13	3.52	2.33	15.88
	BC17	2.01	1.75	18.33
	BG17	3.02	2.1	14.72
24d	**BC14**	2.57	2.11	18.33
	BG14	6.22	3.74	15
	BC18	2.55	1.85	18.67
	BG18	5.13	2.96	14.72
48d	**BC15**	4.32	2.71	18.33
	BG15	8.57	4.83	14.47
	BC19	4.05	2.56	21.15
	BG19	8.38	4.24	14.72
60d	**BC16**	4.61	2.89	17.19
	BG16	13.24	7.11	14.47
	BC20	4.4	2.8	21.54
	BG20	9.68	4.53	14.72

Figure (4), (5) show the load-deflection for carbon, aramid and glass specimens for different diameters 9.50mm, 12.70mm, and 16.00 mm with bond length 12d and 24d respectively. Generally, it is observed that the un-strengthened control beam has lower strength but higher deformation capacity than the strengthened beams. For bond length 12d, the GFRP specimens (BG1, BG5, and BG9) have more deformation capacity than CFRP specimens (BC1, BC5, BC9) and AFRP (BA1, BA5, BA9); the losses in deformation capacity for BG1, BG5, BG9 are 65%, 77% and 77% respectively, for BC1, BC5, BC9 are 80%, 84% and 84% and for BA1, BA5, BA9 are 74%, 79% and 81% respectively with respect to the un-strengthened control beam (table 4). The CFRP specimens have more load-carrying capacity than GFRP and AFRP specimens; as shown in figure (4), by increasing diameter of NSM FRP bars there is an increase in the ultimate load capacity, the percentage of increase in load capacity for BC1, BC5, BC9 are 24%, 30% and 37% respectively, for BG1, BG5, BG9 are 24%, 29% and 37% respectively and for BA1, BA5, BA9 are 26%, 32% and 37% respectively with respect to the un-strengthened control beam.

The results show that with increasing diameter of NSM FRP bars, the ductility index (μΔ) and energy absorption index (EAI) decrease, while the initial stiffness increases. The ductility index (μΔ) for 12.70 mm and 16.00 mm with respect to 9.50 mm is decreased by 18%, 18% in carbon, 31%, 35% in glass and 19%, 33% in aramid respectively, the energy absorption index (EAI) decreased by 29%, 25% in carbon, 46%, 44% in glass and 6%, 26% in aramid respectively, the initial stiffness is increased by 5%, 25% in carbon, 3%, 5%, in glass and 0%, 5% in aramid.

For bond length 24d, the same observation mentioned on curves shown in figure (4) is observed in figure (5). The ratios of increasing in load capacity is increased and become for carbon specimens BC2, BC6, BC10 are 45%, 59% and 90% respectively, for glass specimens BG2, BG6, BG10 are 32%, 32% and 72% respectively, and for aramid specimens BA2, BA6, BA10 are 45%, 52% and 83% respectively. The reduction in deformation capacity for BC2, BC6, BC10 reached to 73%, 81%, 80% respectively, for BG2, BG6, BG10 reached to 57%, 74% , 60% respectively, and for BA2, BA6, BA10 reached to 59%, 75%,75% respectively with respect to the un-strengthened control beam.

The results show that as the bond length increases, the ductility index (μΔ) and energy absorption index (EAI) increase, the initial stiffness increase for carbon while glass and aramid the values are very close to each other. The ductility index (μΔ) for 12.70 mm and 16.00 mm with respect to 9.50 mm is decreased by 36%, 39% in carbon, 42%, 12% in glass and 41%, 42% in aramid respectively, the energy absorption index (EAI) decreased by 39%, 45% in carbon, 40%, 9% in glass and 39%, 41% in aramid respectively, the initial stiffness is increased by 27%, 27% in carbon, 5%, 7%, in glass and 2%, 7% in aramid.

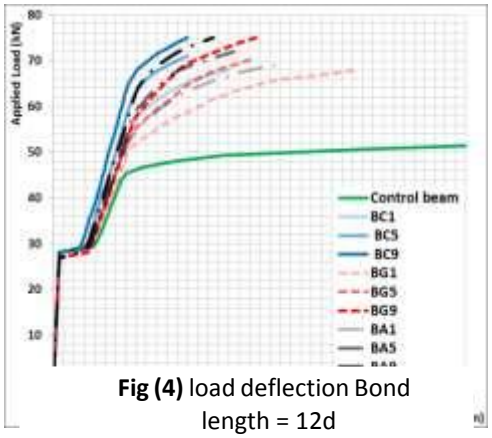

Fig (4) load deflection Bond length = 12d

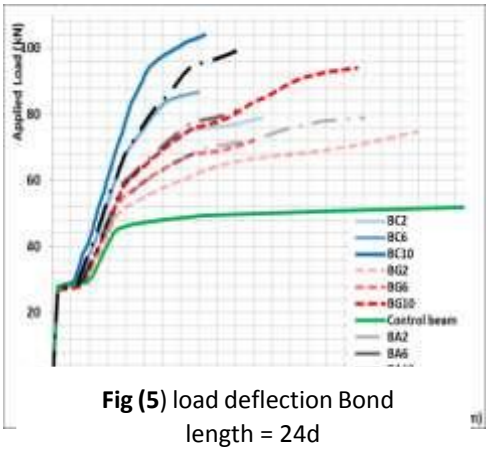

Fig (5) load deflection Bond length = 24d

Figure (6), (7) and shows the load-deflection for carbon, aramid and glass specimens for different diameters 9.50mm, 12.70mm, and 16.00 mm with bond length 48d and 60d respectively.

For bond length 48d, the ratios of increasing in load capacity for carbon specimens BC3, BC7, BC11 reached 71%, 87%, 96%, for aramid specimens BA3, BA7, BA11 reached 61%, 79%, 87% respectively and for glass specimens BG3, BG7, BG11 reached 51%, 76% and 80% respectively. The reduction in deformation capacity reached for BC3, BC7, BC11 67%, 77% , 67%, for BA3, BA7, BA11 51%, 54% 55% respectively and BG3, BG7, BG11 36%, 48% and 55% respectively with respect to the un-strengthened control beam.

The ductility index (μΔ) for 12.70 mm and 16.00 mm with respect to 9.50 mm is decreased by 35%, 5% in carbon, 24%, 34% in glass and 8%, 14%in aramid respectively, the energy absorption index (EAI) decreased by 39%, 9% in carbon, 20%, 34% in glass and 1%, 20 % in aramid respectively, the initial stiffness is increased by 33%, 43% in carbon, 2%, 4%, in glass and 5%, 7% in aramid.

For bond length 60d, The same behavior is observed, with increasing the bond length, the ratios of increasing in load carrying capacity increased and reached for BC4, BC8, BC12 76%, 92% and 119% respectively, for BA4, BA8, BA12 68%, 83% and 96% respectively and for BG4, BG8, BG12 68%, 76% and 92% respectively with respect to the un-strengthened control beam. The reduction in deformation capacity for BC4, BC8, BC12 are 63%, 72%, 57% respectively, for BA4, BA8, BA12 are 32%, 39%, 53% respectively and for BG4, BG8, BG12 are 22%,28% and 53% respectively.

The ductility index (μΔ) and the energy absorption index (EAI) decreased as the FRP diameter increased, it is observed at diameter 12.70mm both ductility index and energy absorption index decreased with respect to diameter 9.50mm by 25% and 38% respectively in carbon, 18% and 19% respectively in glass, and 11% and 6% respectively in aramid, for 16.00mm diameter the decreasing are 9% and 3% respectively in carbon, 43% and 46% respectively glass, and 36% and 37% respectively in aramid.

The initial stiffness for diameter to 12.70mm and 16.00mm leads is increased with respect to diameter 9.50mm by 31%, 43% respectively in carbon, 0%, 7% respectively in glass and 2%, 11% respectively in aramid.

4.3 FRP tensile stress results

Figures (8), (9), (10), and (11) show the load-stress curves for carbon, aramid and glass specimens for diameters 9.50 mm, 12.70 mm, and 16.00 mm with bond length 12d, 24d, 48d, and 60d respectively. It is observed that, for all types of FRP bars, as the bond length of NSM bar increases, the bar tensile stress and the ultimate load capacity increases. For bond length 12d, the ratio of actual tensile stress to ultimate tensile stress for carbon specimens BC1, BC5, BC9 are 27%, 30%, 25% respectively, for glass specimens BG1, BG5, BG9 are 53%, 32%, 28% respectively, and for aramid specimens BA1, BA5, BA9 by approximately are 29%, 22% and 16% respectively.

For bond length 24d, the ratio of actual tensile stress to ultimate tensile stress for carbon specimens BC2, BC6, BC10 by approximately are 49%, 51% and 47% respectively, for glass specimens BG2, BG6, BG10 by approximately are 74%, 40% and 55% respectively, and for aramid specimens BA2, BA6, BA10 by approximately are 57%, 35% and 35% respectively.

For bond length 48d, the ratio of actual tensile stress to ultimate tensile stress for carbon specimens BC3, BC7, BC11 by approximately are 68%, 76% and 70% respectively, for glass specimens BG3, BG7, BG11 by approximately are 107% , 79% and 67% respectively, and for aramid specimens BA3, BA7, BA11 by approximately are 71%, 57% and 48% respectively.

For bond length 60d, the ratio of actual tensile stress to ultimate tensile stress for carbon specimens BC4, BC8, BC12 by approximately are 76 %, 86% and 86% respectively, for glass specimens BG4, BG8, BG12 by approximately are 128%, 93% and 71% respectively, and for aramid specimens BA4, BA8, BA12 by approximately are 87%, 78% and 49% respectively.

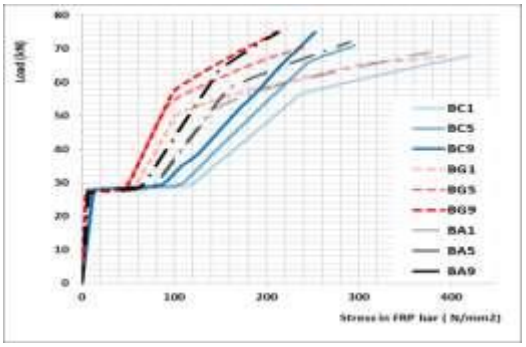

Fig (8) load stress Bond length = 12d

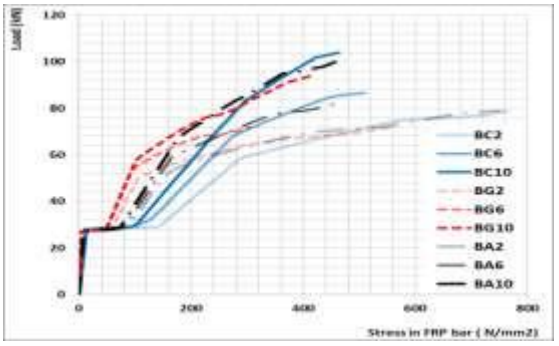

Fig (9) load stress Bond length = 24d

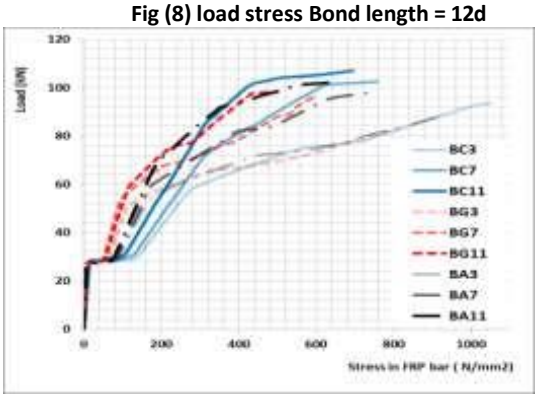

Fig (10) load stress Bond length = 12d

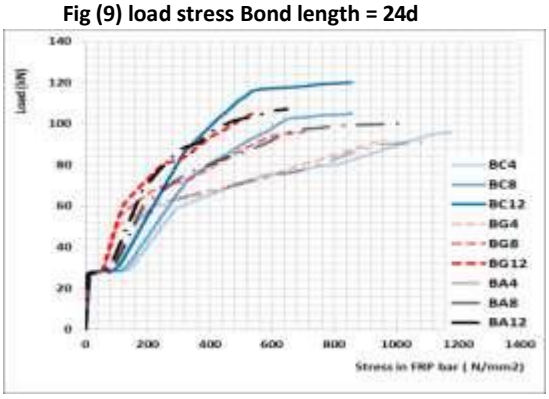

Fig (11) load stress Bond length = 24d

4.4 Effect of Type and Number of NSM FRP Bars

To study the effect of type and number of NSM FRP bars on flexural response and failure mode of the different models, twenty-four models of two types of fibers (fiber carbon (CFRP) and glass fiber (GFRP)) were studied, with constant other parameters such as diameter of strengthened NSM FRP bars and bond length.

It is observed that increasing number of NSM FRP bars lead to little increase in the ultimate load capacity and little decrease in deformation capacity due to little enhancements of bond resistance. As the bond length increase, the number of bars has more effect in increasing in the ultimate load capacity. Figure (12), (13) show the load-deflection curve for carbon and glass specimens at diameter 9.50mm by using one bar, two bars and three bars with bond length 12d and 24d respectively. For bond length 12d, there is an increase in the load carrying capacity.

For carbon specimens BC1, BC13, BC17 by approximately 24%, 28% and 26% and for glass specimens BG1, BG13, BG17 by approximately 24%, 28% and 28% respectively than the un-strengthened control beam. But the loss in deformation capacity for carbon specimens BC1, BC13, BC17 by approximately 80%, 85% and 86% and for glass specimens BG1, BG13, BG17 by approximately 65%, 78% and 80% than the un-strengthened control beam.

For bond length 24d, basically same observation mentioned on curves shown in Figure (12) with increasing in ratio of capacity are observed in Figure (13). The ratios of increasing in load carrying capacity for BC2, BC14, and BC18 by approximately 45%, 54% and 52% and for BG2, BG14, BG18 by approximately 32%, 46% and 52% respectively than the un- strengthened control beam. And the reduction in deformation capacity for BC2, BC14, and BC18 by approximately 73%, 80% and 83% and for BG2, BG14, BG18 by approximately 57%, 66% and 72% respectively than the un-strengthened control beam.

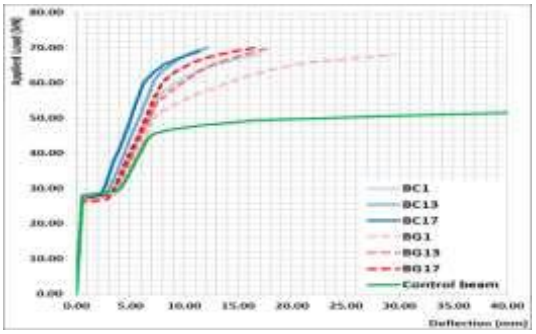

Fig (12) load deflection Bond length = 12d

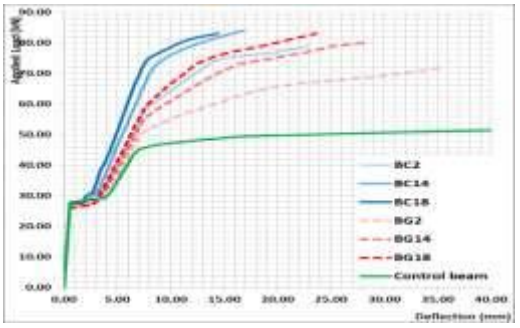

Fig (13) load stress Bond length = 24d

Figure (14) and (15) shows the load-deflection curve for carbon and glass specimens at diameter 9.50mm by using one bar, two bars and three bars with bond length 48d and 60d respectively. Basically same observation mentioned on curves shown in figure (12) are observed in figure (14) but the ratios of increasing in load carrying capacity for carbon specimens BC3, BC15, BC19 by approximately 71%, 87% and 110% and for glass specimens BG3, BG15, BG19 by approximately 51%, 72% and 76% respectively than the un strengthened control beam. And the reduction in deformation capacity for carbon specimens BC3, BC15, BC19 by approximately 67%, 74% and 75% and for glass specimens BG3, BG15, BG19 by approximately 36%, 54% and 59% respectively than the un–strengthened control beam. For bond length 60d, the ratios of increasing in load carrying capacity for carbon specimens BC4, BC16, BC20 by approximately 76%, 98% and 110% and for glass specimens BG4, BG16, BG20 by approximately 68%, 74% and 79% respectively than the-un strengthened control beam. And the reduction in deformation capacity for carbon specimens BC4, BC16, BC20 by approximately 63%, 70% and 73% and for glass specimens BG4, BG16, BG20 by approximately 22%, 32% and 56% respectively than the un-strengthened control beam.

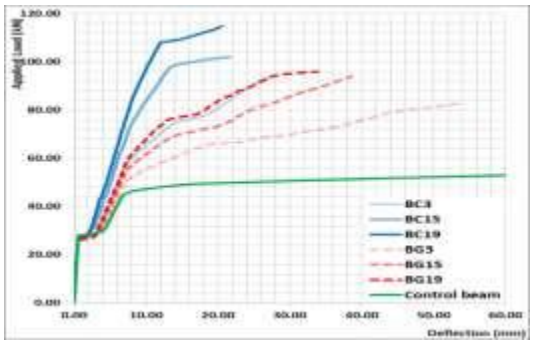

Fig (14) load deflection Bond length = 48d

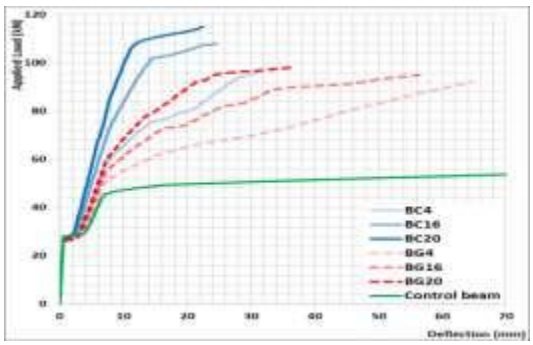

Fig (15) load stress Bond length = 60d

Table 5 show with increasing number of NSM FRP bars for carbon or glass; there is a decrease in both ductility and energy absorption index (EAI). For bond length 12d, 24d, 48d, and 60d, the reduction in ductility with respect to one bar, for two bars CFRP are 38%, 31%, 26%, 26% respectively, and EAI are 36%, 46%, 35%, 41% respectively. For three bars
CFRP, the reduction in ductility are 44%, 39%, 30%, 28% respectively, and EAI are 35%, 46%, 39%, 44% respectively. For bond length 12d, 24d, 48d, and 60d, the reduction in ductility for two bars GFRP are 23%, 21%, 32%, 18% respectively, and EAI are 47%, 26%,
40%, 33% respectively. For three bars GFRP, the reduction in ductility are 17%, 43%, 40%, 48% respectively, and EAI are 55%, 39%, 42%, 51% respectively. With increasing number of NSM FRP bars for carbon or glass, there is an increase in the stiffness. For bond length 12d, 24d, 48d, and 60d, the % of increase in initial stiffness of two and three bars with respect to one bar for both carbons are (21%, 29%), (29%, 31%), (29%, 48%) and (21%, 51%) respectively. for glass, the initial stiffness of two and three bars are (15%, 7%), (11%, 9%), (7%, 9%) and (7%, 9%) respectively.

5.Effect of Number of NSM FRP Bars with Equal Reinforcement Ratio

To study the number of FRP bar with constant FRP reinforcement ratio (3 bars 9.50mm diameter approximately equal 1 bar 16.00mm diameter) on flexural response of the different models, sixteen models of two types of fibers were studied using ANSYS. Other parameters such as type of NSM FRP bars and bond length were constants for those models. Figure (16) and (17) show the load-capacities and deformation capacity respectively for carbon and glass specimens with bar 16.00mm diameter by using one bar and 3bars of 9.50mm diameter with approximately the same FRP reinforcement ratio with bond length 12d, 24d, 48d, and 60d. It is observed that with increasing bond length in carbon or glass specimens, there is an increase in the ultimate load capacity and deformation capacities. Also using one bar with diameter16.00 mm demonstrate increasing in the load-carrying capacity and deformation capacities than using 3 bars with diameter 9.50mm.

For bond length 12d, there is an increase in the load-carrying capacity for carbon specimens BC9, BC17 by approximately 37%, 26% and for glass specimens BG9, BG17 by approximately 37%, 28% respectively than the un-strengthened control beam. But the losses in deformation capacity for carbon specimens BC9, BC17, by approximately 84%, 86% and for glass specimens BG9, BG17 by approximately 76%, 80% than the un-strengthened control beam. For bond length 24d, there is an increase in the load-carrying capacity for carbon specimens BC10, BC18 are 90%, 52% and for glass specimens BG10, BG18 are 72%, 52% than the un-strengthened control beam. But the losses in deformation capacity for carbon specimens BC10, BC18, by approximately 80%, 83% and for glass specimens BG10, BG18 by approximately 60%, 72% than the un-strengthened control beam. For bond length 48d, there is an increase in the load-carrying capacity for carbon specimens BC11, BC19 by approximately 96%, 110% and for glass specimens BG11, BG19 by approximately 80%, 76% respectively than the un-strengthened control beam. The losses in deformation capacity for carbon specimens BC11, BC19, by approximately 67%, 75% and for glass specimens BG11, BG19 by approximately 55%, 59% than the un-strengthened control beam. For bond length 60d, there is an increase in the load-carrying capacity for carbon specimens BC12, BC20 by approximately 119%, 110% and for glass specimens BG12, BG20 by approximately 92%, 79% respectively than the un-strengthened control beam. the losses in deformation capacity for carbon specimens BC12, BC20, by approximately 57%, 73% and for glass specimens BG12, BG20 by approximately 53%, 56% than the un-strengthened control beam.

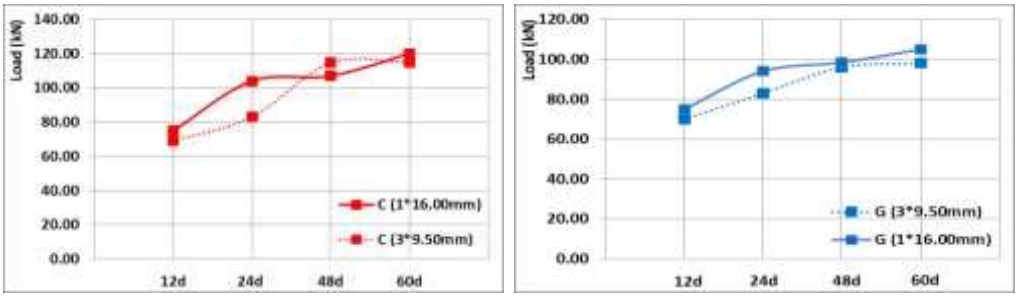

Fig (16) Load-capacities for one bar with diameter 16.00 mm specimens and 3 bars with diameter 9.50mm specimen

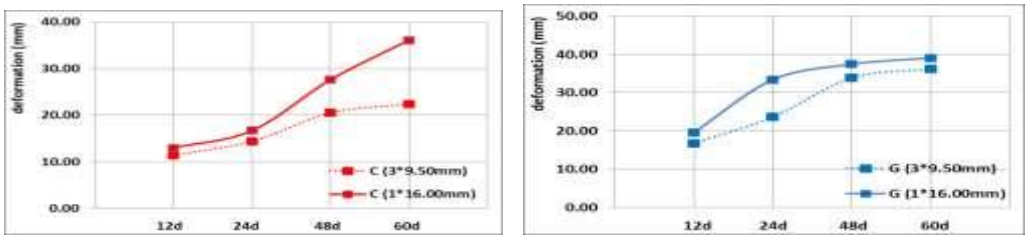

Fig (17) deformation-capacities for one bar with diameter 16.00 mm specimens and 3 bars with diameter 9.50mm

specimen

Figure (18) shows the ductility and EAI for carbon and glass specimens with bar diameter 16.00mm by using one bar and 3bars of 9.50mm diameter with approximately the same FRP reinforcement ratio with bond length 12d, 24d, 48d, and 60d. It is observed that with increasing bond length of FRP NSM bars, the ductility and EAI increase. Also using one bar with diameter 16.00 mm shows an increase in the ductility index and EAI than using 3 bars with diameter 9.50mm.

For bond length 12d with three bars 9.50mm in diameter, there is a decreasing in ductility with 0% in carbon and 14% in glass with respect to one bar 16.00mm in diameter; also EAI has decreased by 13% in carbon and 19% in glass, for bond length 24d the decreasing in ductility is 0% in carbon and 29% in glass and for EAI is 3% in carbon and 33% in glass. With increasing bond length, the ratio of decreasing in ductility is increased for carbon and become 26% and 34% for 48d and 60d respectively, while for EAI, the ratio is 33% and 42% respectively. It can be noted, for bond length 48d and 60d, the ratio of decreasing for both ductility index and EAI is insignificant and not more than 10%.

All specimens have close elastic stiffness with small difference and be neglected for different bond length and FRP type.

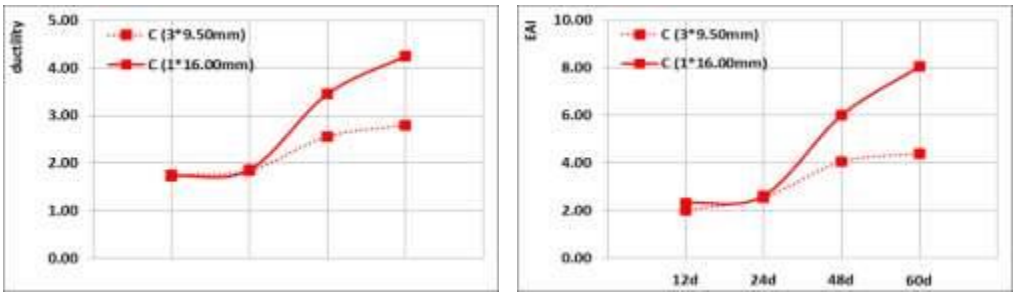

Fig (18) Ductility and EAI for one bar with diameter 16.00 mm specimens and 3 bars with diameter 9.50mm specimen

5. CONCLUSION

This study's conclusions can be summarized as follows:

- The un- fortified control beam has lower strength but higher deformation capacity than the fortified beams.
- Debonding, which appears as concrete cover splitting at the level of the steel reinforcement, is the mode of failure for the strengthened beams. The mode of failure for the strengthened beams is debonding in the form of concrete cover splitting at the level of the steel reinforcement.
- The initial stiffness, ultimate load capacity, deformation capacity, and energy absorption index (EAI) of NSM FRP bars generally increase with bond length; this rise is particularly pronounced for bond lengths of at least 48 times the bar diameter.
- The ductility index (μΔ), energy absorption index (EAI), and initial stiffness all rise as
- the diameter of NSM FRP bars increases.
- Because of the increased bond resistance, adding more FRP NSM bars with the same reinforcement ratio has led to a little gain in ultimate load capacity and a decrease in deformation capacity.
- As the number of NSM FRP bars increases, stiffness and the energy absorption index (EAI) decrease. Additionally, compared to utilizing three bars with a diameter of 9.50 mm, employing one bar with a diameter of 16.00 mm has an increased capacity for load carrying, deformation, and EAI.

REFERENCES

1. ACI Committee 440, "Guide for the design and construction of externally bonded FRP systems for strengthening concrete structures," (ACI 440.2R-02). Technical report, American Concrete Institute, Farmington Hills, Michigan, 2002.
2. De Lorenzis L., Nanni A., and La Tegola, "Flexural and shear strengthening of reinforced concrete structures with Near Surface Mounted FRP rods," Proceeding of the 4th international Conference on Advanced Composites Materials in Bridges and Structures (ACMBS 2000), J.L. Humar and A.G Razagpur Editors, Canadian Society for Civil Engineering, Ottawa, pp 521-528 (2000).
3. EL – Hacha R., Filho D. S., Melo G. S., and Rizkalla S. H, "Effectiveness of Near Surface Mounted FRP Reinforcement for Flexural strengthening of Reinforced Concrete Beams," Proceeding of the 4th international Conference on Advanced Composites Materials in Bridges and Structures (ACMBS 2004), Calgary, Ontario, Canada, July 20- 23, 2004.
4. Hollaway M.A. and Raoof M, "Strengthening of Reinforced Concrete Structure," CRC press, 2001.
5. J. F. Chen and J. G. Teng. "Anchorage strength models for FRP and steel plates bonded to concrete," Journal of structural Engineering, vol. 127, no. 7, pp. 784-791, 2001.
6. Jeevan N, Keerthi Gowda B.B., Archana D.P., Abdul Razak, Abbas M. and Ahamed S.C. "Experimental study on flexural strengthening of RC beams with NSMtechnique by different orientation of CFRP laminate," Ain Shams Engineering Journal, Volume 14, Issue 1, 2023.
7. Kang J. Y., Park Y. H., Park J. S., You Y. J., and Jung W. T, "Analytical Evaluation of RC beams strengthened with near surface mounted CFRP laminates," American Concrete Institute (ACI), Special Publication, vol. 230, no. 45, pp. 779-794, 2005.
8. L. De Lorenzis and J.G. Teng. "Near surface mounted FRP reinforcement: An emerging technique for strengthening structures," Composite Part B: Engineering, vol. 38, no. 2, pp. 119-143, 2007.
9. M. Tavakkolizadeh, "Strengthening and repair of steel U concrete composites girders using CFRP laminates, "PhD Thesis University of Arizona, 2001.
10. R.Parretti and A. Nanni, "Strengthening of RC members using near surface mounted FRP composites: Design overview," Advanced in Structural Engineering, vol. 7, no. 6, pp. 469-483, 2004.
11. S. Yang, K.Park, and W. Neale, "Flexural behavior of reinforced concrete beams strengthened with prestressed carbon composites," Composite Structures, vol. 88, pp. 497-508, 2009.
12. S.M. Soliman, E. El-Salakawy, B. Benmokrane, "Flexural behavior of concrete beams strengthened with near surface mounted FRP bars," Fourth International Conference on FRP Composites in Civil Engineering (CICE2008), Zurich, Switzerland, pp 22-24, July 2008.
13. S.O. Asplund, "Strengthening bridge slabs with grouted reinforcement," Journal of the American Concrete Institute, vol. 20, no. 2, pp. 397-406, 1949.
14. Sabau C., Popescu C, Sas G, W. S. Jacob, B. Thomas and T. Björn, "Strengthening of RC beams using bottom and side NSM reinforcement," Composites Part B: Engineering, Volume 149, Pages 82-91, 2018
15. Szczech D., Krawczyk L. and Kotynia R "Flexural strengthening of RC beams with NSM CFRP laminates," 10th International Conference of Advanced Models and New Concepts in Concrete and Masonry Structures (AMCM 2020), Volume 323, Lublin, Poland, October 21-23, 2020.